Asian Journal of Chemistry; Vol. 34, No. 3 (2022), 673-680

ASIAN JOURNAL OF CHEMISTRY

https://doi.org/10.14233/ajchem.2022.23578

Photocatalytic Degradation of Rhodamine B Dye by Using Tin-Doped CeO_2-Fe_2O_3 Nanocomposite

H.S. AL-SHEHRI[1], M.S. PATEL[2], S. ALWERA[3], V.S. TALISMANOV[4], V. ALWERA[3,*] and R.R. MACADANGDANG JR.[5]

[1]Chemistry Division, King Khaled Military Academy, SANG, 11495, Riyadh, Saudi Arabia
[2]Mohammed Al-Mana College for Medical Sciences, Dammam 4222, Saudi Arabia
[3]Department of Chemistry, Indian Institute of Technology Roorkee, Roorkee-247667, India
[4]Depatment of Chemistry, Moscow Institute of Physics and Technology, Dolgoprudny, Moscow Region, 141701, Russian Federation
[5]Department of Medical Technology, Institute of Arts and Sciences, Far Eastern University, Manila, Philippines

*Corresponding author: E-mail: alweravijay@gmail.com

Received: 9 October 2021; *Accepted*: 17 December 2021; *Published online*: 14 February 2022; AJC-20702

Organic dyes are frequently used in various industries such as textiles, medicines, plastics, *etc.* and contribute as a major source of environmental pollutants, which leads to harmful effects on livings. Therefore, in this study, a Sn-doped CeO_2-Fe_2O_3 photocatalyst was synthesized using the thermal decomposition method and applied for the effective degradation and removal of rhodamine B dye under solar irradiation. The as-synthesized catalyst was characterized by powder X-ray diffraction (XRD), field-emission scanning electron microscopy (FE-SEM), Brunauer-Emmett-Teller (BET) and UV-vis diffuse reflectance (UV-vis DRS) techniques. The particle size of the photocatalyst was found 1-2 µm with a high surface area. The band gap energies of the catalyst narrowed to 2.2 eV after the Sn doping. The doping of Sn^{4+} ions into CeO_2 lattice leads to the enhanced photocatalytic activity of CeO_2-Fe_2O_3 composite by modified the Fermi levels of catalyst. The catalyst has shown a fast degradation rate under solar irradiance and is able to perform complete degradation of rhodamine B dye. The photocatalyst showed the COD removal up to 96% from the dye solution. Further, the scavenger test revealed the active species hydroxyl ($^{\bullet}OH$) and superoxide ($O_2^{\bullet-}$) radical are involved in the degradation of rhodamine B dye. The complete degradation of rhodamine B dye was studied and confirmed by high-performance liquid chromatography. A plausible mechanism is proposed for the degradation process and charge transfer during the degradation.

Keywords: Metal oxides, Photocatalyst, Degradation, Rhodamine B, HPLC, COD.

INTRODUCTION

Recently, the development of industrialization and urbanization has grown very fast to fulfil the requirements and needs of mankind. Although the growth in these areas is necessary but it is leading to a major problem, environmental pollution. The continuous discharge from industries causing damage to the living and environment. The industrial waste includes different types of pollutants such as oils, pharmaceuticals, radioactive waste, cosmetics, photochemical, textiles discharge, *etc.* [1,2]. The release of these pollutants into the water bodies and soil polluted the drinking water, groundwater and river streams. When this polluted water is exposed to living organisms, it causes many harmful effects on animals, aquatic animals, plants and humans, such as carcinogenic, mutagenic effects. Among different industrial wastes, organic dyes are one of the major sources for the water pollution as it is highly used in textile, leather, paint, food industries, *etc.* [3-7]. Approximately hundreds of dyes are commercially used in different industries, which includes biodegradable and non-biodegradable dyes [8-10]. The non-biodegradable dyes sustain in the environment and water bodies for a long time and cause harmful effects on living organisms continuously [11]. Textile dyes contain organic and inorganic constituents, which are hard to remove or degrade by traditional water treatment methods [12,13].

Traditional water treatment methods such as coagulation, membrane filtration, reverse osmosis, *etc.* are found to be less or non-effective on the removal of organic dyes [14]. Thus, researchers are highly interested in the development of technologies, which are capable of degradation and removal of dyes such as chlorination, ozonation, adsorption, biodegradation, catalytic/photocatalytic degradation, *etc.* Among these various

degradation processes, photocatalytic degradation has its own significance because it is capable of complete removal of organic dyes, pharmaceutical compounds, *etc*. [15]. The photocatalytic activity is shown by semiconductor materials that have sufficient band gap in order to degrade pollutants, *e.g.* metal oxides, nitrides, sulfides [16,17]. Among different metal oxides, TiO_2, ZnO, CuO, CeO_2, Fe_3O_4, Fe_2O_3, $BiVO_4$, *etc*. are well known for their photocatalytic and catalytic activity, energy storage, fuel cells, water splitting, *etc*. [15,18-21].

The photocatalysis process is highly dependent on values such as band gap energies, charge transfer efficiency, photocorrosion. Large band gap and low charge transfer limit the efficiency of a photocatalyst, so the challenge is to overcome these limitations for better activity. One of the solutions to resolve these limitations is to develop hetero-junctions. Heterojunction can be developed by doping metals or non-metals in the composite and it is found helpful to minimize the band gap energies and increase the charge transfer efficiency [22,23]. Many researchers are interested in fluorite structured CeO_2 metal oxide systems due to their high efficiency in solar cells, fuel cell, sensors and high thermal-chemical stability [24,25]. But CeO_2 has a large band gap of 3.2 eV, so it does not show activity under the solar irradiance. For this purpose, CeO_2 is mixed or combined with different metals or metal oxides to enhance the degradation efficiency, *e.g.* CeO_2-TiO_2, CeO_2-Cu_2O, CeO_2-$BiVO_4$, CeO_2-Bi_2O_3, CeO_2-ZnO, CeO_2-ZnO-TiO_2, CeO_2-α-MoO_3 [12-15,26-28]. To modify the band gap of CeO_2 for photocatalysis, we must choose a metal oxide having low band gap values such as Fe_2O_3. Fe_2O_3 is found to have a low band gap and high visible light absorptivity and in a system with the combination of other metal oxides, Fe_2O_3 is found active under solar irradiance [29,30].

In this work, we synthesized a doped mixed metal oxide system for photocatalytic degradation of organic dyes under solar irradiation. Here, Fe_2O_3 with high visible light absorptivity is mixed with CeO_2 and the synthesized composite was found active towards the degradation of dyes under sunlight. Along with this, Sn^{4+} is doped into CeO_2-Fe_2O_3 composition to achieve optimum charge concentration at the catalyst surface. The doping of Sn^{4+} leads to the modification in band position and enhance charge separation as it occupied Ce^{4+} sites in the lattice [31,32]. The phase and structural properties of the photocatalyst was studied by XRD, SEM and the surface area was measured by BET surface analysis. The degradation studies of rhodamine B dye by both Sn doped and undoped catalyst revealed that Sn doped catalyst was found more active towards the degradation of rhodamine B dye. Further, the photocatalytic process was understood and explained by studying the scavenge test, doses test, pH test and recycling test. The HPLC analysis was helpful in order to identify the intermediate molecules [33,34].

EXPERIMENTAL

$FeCl_3$ of analytical grade was purchased from Sigma-Aldrich, USA. $Ce(NO_3)_2{\cdot}6H_2O$ and $SnCl_4{\cdot}5H_2O$ of analytical grade were purchased from Alfasar. For the synthesis of Sn-doped CeO_2-Fe_2O_3 composite, a thermal decomposition method was used. A solutions of $FeCl_3$ and $Ce(NO_3)_2{\cdot}6H_2O$ were taken in a 1:2 molar ratio, while $SnCl_4{\cdot}5H_2O$ was used 5% of the total mass. Then, all measured chemicals were dispersed in 100 mL isopropanol. The mixture was allowed to stir magnetically on a magnetic stirrer at 85 ºC until it got dry. Then the obtained powder was heated for 1 h at 120 ºC in a vacuum oven. After this, the compound was grounded in a mortar pestle for 1 h and then placed in a muffle furnace for 2 h at 450 ºC for calcination [29,35,36]. The resulting compounds were then analyzed for further study.

Photocatalytic activity: For the photocatalytic activity, all the experiments were performed under sunlight irradiation in the month of April to July. First, 100 mg of catalyst was taken in a 250 mL beaker with 100 mL of dye solution (1×10^{-5} M) at desired pH. The pH of the dye solutions was adjusted by dil. HCl and NaOH. Then the above solution was stirred for 3 h to reach the adsorption-desorption equilibrium and the beaker was placed under direct sunlight. The change in the concentration of the dye solution was measured by taking 3 mL of aliquots from the beaker after a certain time period. For this purpose, the aliquots were first centrifuged at 10,000 rpm and then UV-vis spectrum was recorded. The degradation efficiency of the catalyst was calculated according to the following equation:

$$\text{Degradation efficiency } (\%) = \frac{C_o - C}{C_o} \times 100$$

where C_o and C are the initial and final absorbance of the dye solutions [30]. After the photocatalytic experiment, the recovered catalyst was again used for the next cycle. The photocatalyst was tested for four consecutive cycles.

Characterization: The X-ray powder diffraction (XRD) was recorded by using a Bruker AXSD8 Advance diffractometer (Cu-Kα1; λ = 1.5406 Å). Field emission scanning electron microscopy (FESEM) was recorded by using Zeiss, Ultra plus55. Brunauer-Emmett-Teller (BET) surface area measurement of the compound was performed by using NOVA 2200e instrument. The Diffuse Reflectance Spectra (DRS) was recorded on the Shimadzu UV-2450 spectrophotometer. The pH of the dye solutions was measured by a pH meter (Eutech pH 700).

Chemical oxygen demand (COD): The COD of the dye solution was measured by using a digestion unit (DRB 200) and UV-vis spectrophotometer. The COD sample aliquots were collected after a certain time interval and then centrifuged at 10,000 rpm for 10 min.

High-performance liquid chromatography (HPLC): HPLC analysis was done by using Shimadzu LC-2010AHT along with the C_{18} column [37]. Acetonitrile and water (1:1), H_3PO_4 (50 mM), at 3.5 pH were used as the mobile phase and operated in gradient mode [38]. The HPLC was recorded by collecting 3 mL reaction aliquots were collected after a time interval. The sample aliquots were first centrifuged in order to remove the catalyst particles and then filtered through a 45 m syringe filter.

Detection of reactive species: To identify the reactive species involved in the photocatalytic degradation, scavenger tests were performed. For this, a suitable scavenger was added

to the catalyst-dye solution and photocatalytic experiments were performed similarly as earlier. The scavengers used are benzoquinone (BQ) for $O_2^{\bullet-}$, ammonium oxalate (AO) for h^+ and *tert*-butanol (*t*-BuOH) for $^{\bullet}OH$ scavenging.

RESULTS AND DISCUSSION

The crystallite phase of the Sn-doped CeO_2-Fe_2O_3 composite was identified by X-ray diffraction studies. Fig. 1 shows the XRD patterns of CeO_2-Fe_2O_3 (Fig. 1a) and Sn-doped CeO_2-Fe_2O_3 (Fig. 1b). In Fig. 1a, the XRD peaks obtained at 2θ = 27.2º, 28.99º, 33.39º, 47.91º, 56.75º, 69.60º, 79.47º corresponding to (012), (111), (200), (220), (311), (400) and (420) planes, respectively, which confirmed the phase of CeO_2 having fluorite structure [JCPDS# 00-034-0394] [39]. On the other hand, remaining XRD peaks at 25.1º, 35.4º, 49.7º, 54.9º and 62.1º, correspond to (101), (110), (024), (116) and (214) crystal planes, respectively, indicate the phase of Fe_2O_3 having rhombohedral phase [40]. The XRD pattern shown in Fig. 1b is also found to have a similar XRD pattern as CeO_2-Fe_2O_3, which indicates that doped Sn^{4+} is incorporated well in the structure. But all the peaks are found shifted towards the higher 2θ values compared to the Sn undoped sample that is due to the interaction of Sn^{4+} with Ce and Fe in the crystal structure. Here, Sn^{4+} has formed SnO_2 by replacing Ce^{4+} from the CeO_2 lattice and the resulting Sn doped CeO_2 lattice is formed. This Sn doped CeO_2 lattice interacted with Fe_2O_3 and caused the shift in the XRD peaks.

Fig. 2a shows the FESEM analysis of the as-synthesized Sn doped CeO_2-Fe_2O_3 composite. The image shows the catalyst nanoparticles have sphere-shaped morphology having a rough surface with irregular size. The spheres are found to have the varying size in the range of 1-2 mm particle size.

The surface area of the catalyst was studied by BET analysis and the N_2 adsorption-desorption isotherm curve is shown in

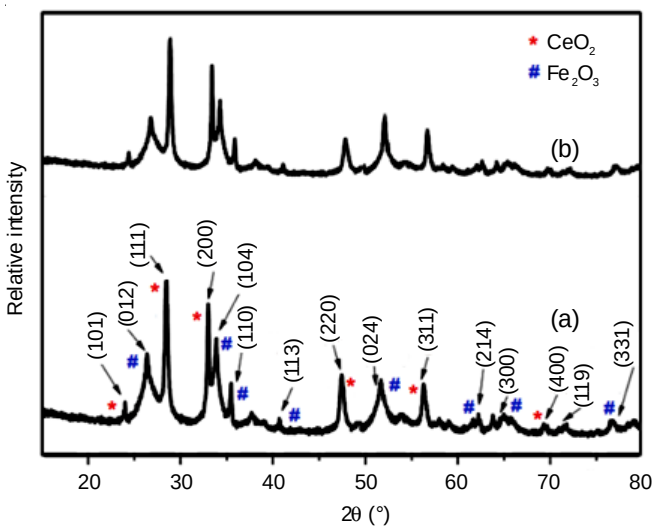

Fig. 1. XRD pattern for (a) CeO_2-Fe_2O_3 and (b) Sn doped CeO_2-Fe_2O_3

Fig. 2b. In this figure, both the catalyst are found to have a typical type IV isotherms curve [41]. The surface area of Sn doped CeO_2-Fe_2O_3 catalyst was found 24.2 m^2/g, while the CeO_2-Fe_2O_3 composite has 17.4 m^2/g surface area, which is very less than that of the Sn doped catalyst.

The UV-visible DRS spectra for the composite are shown in Fig. 3. The spectra show a wide absorption edge in the visible region for both composites and the absorption edge appeared above 400 nm (Fig. 3a) [42-44]. Nanocomposite CeO_2-Fe_2O_3 shows strong absorption around 500 nm and narrowing near about 600 nm; on the other hand, an extreme change was observed after the doping of Sn^{4+}. The Sn^{4+} doped sample showed a high absorption edge with the shift toward the higher wavelength region near about 600 nm. The significant absorption edge of the Sn doped composite shows the high absorptivity for the visible light, which leads to a high degradation

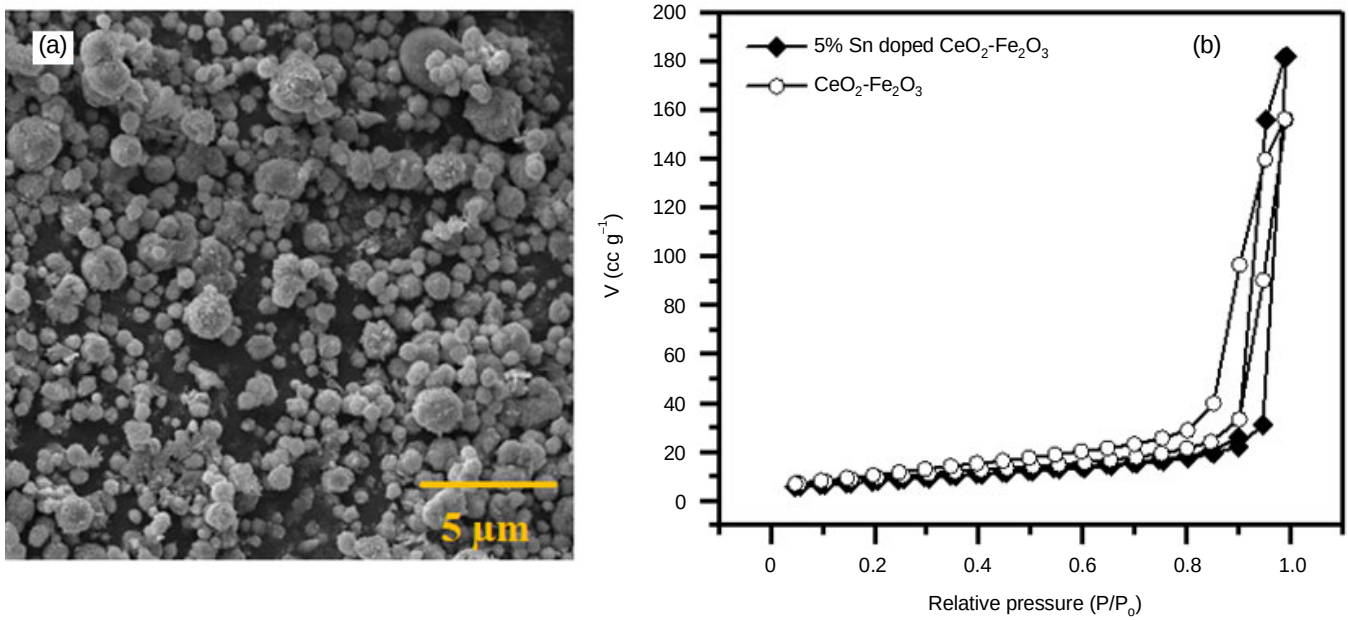

Fig. 2. (a) FESEM image of the synthesized Sn doped CeO_2-Fe_2O_3 composite. (b) The BET surface area of CeO_2-Fe_2O_3 and Sn doped CeO_2-Fe_2O_3 composites

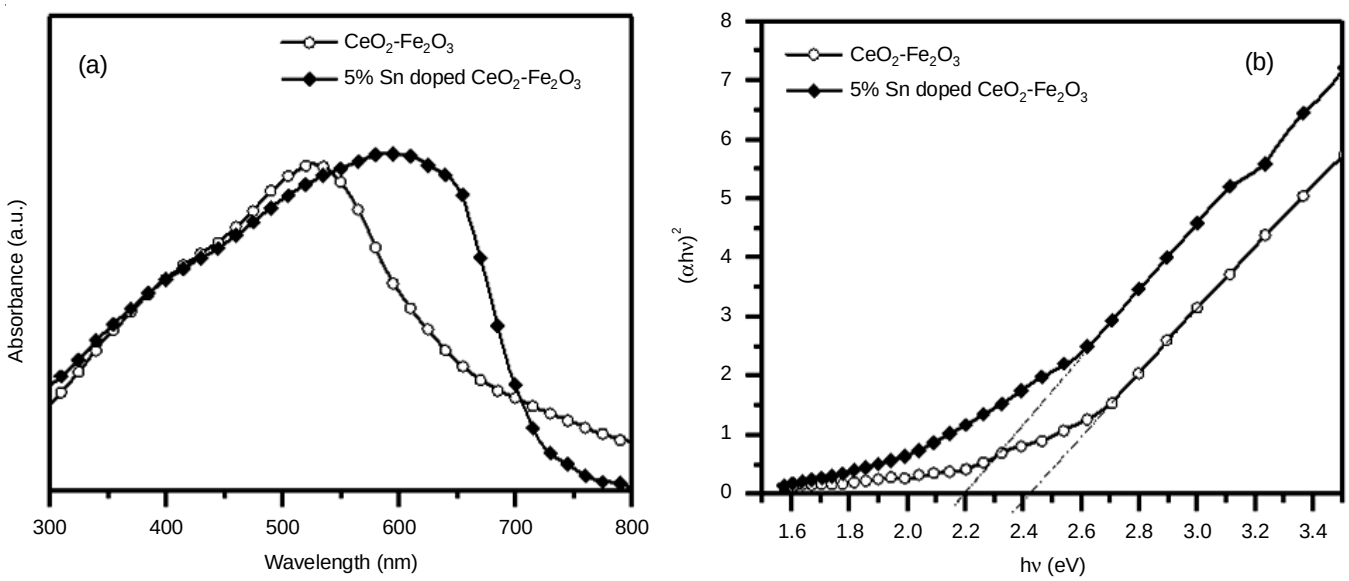

Fig. 3. DRS studies for CeO_2-Fe_2O_3 and Sn doped CeO_2-Fe_2O_3; (a) UV-visible absorbance spectra and (b) Tauc plot

rate. Fig. 3b represents the Tauc plot for the bang gap energies for both Sn doped and undoped composites. The direct band gap value for the CeO_2-Fe_2O_3 sample was found 2.4 eV, but the doping of Sn^{4+} caused the change in the band gap value, as it decreased to 2.21 eV.

Photocatalytic degradation of rhodamine B dye: The photocatalytic activities of Sn doped CeO_2-Fe_2O_3 and CeO_2-Fe_2O_3 samples were studied by using rhodamine B dye (pH = 10) as a sample pollutant under sunlight irradiance. Fig. 4 shows the photocatalytic degradation efficiency of Sn doped CeO_2-Fe_2O_3 and CeO_2-Fe_2O_3 catalyst. Here, Sn doped CeO_2-Fe_2O_3 catalyst showed approximately 98% degradation of rhodamine B dye solution within 100 min; on the other hand, the CeO_2-Fe_2O_3 sample shows only 60% degradation of rhodamine B dye. The high degradation rate of rhodamine B dye by Sn doped CeO_2-Fe_2O_3 is due to a lower band gap than that of the CeO_2-Fe_2O_3 sample.

After that the photocatalytic degradation of rhodamine B dye with Sn doped CeO_2-Fe_2O_3 was studied by the effect of

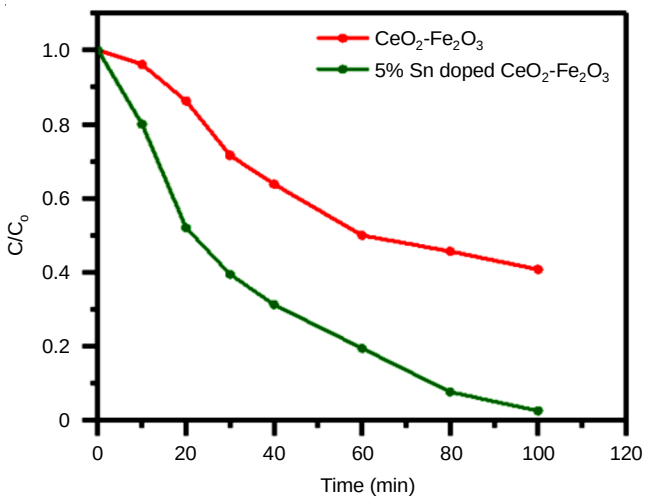

Fig. 4. Photocatalytic degradation of rhodamine B dye with time by CeO_2-Fe_2O_3 and Sn doped CeO_2-Fe_2O_3

catalyst doses (Fig. 5) [45]. The doses of catalyst were varied from 50 to 150 mg/L while the concentration of rhodamine B dye solution was remained constant (1×10^{-5} M). Here, the rate of photocatalytic degradation increased as the concentration of catalyst increased. Fig. 5 indicates when the concentration of the Sn doped catalyst was 0.5 g/L, the catalyst was able to remove about 58% of rhodamine B dye from the solution in 100 min. Further increase in the concentration of catalyst leads to the high degradation rate of rhodamine B dye, as 0.8 g/L of catalyst is able to degrade 81% of rhodamine B dye from solution and 1.5 g/L of catalyst removed 99% rhodamine B dye within 40 min. So, the degradation rate of rhodamine B dye is directly proportional to the concentration of the catalyst.

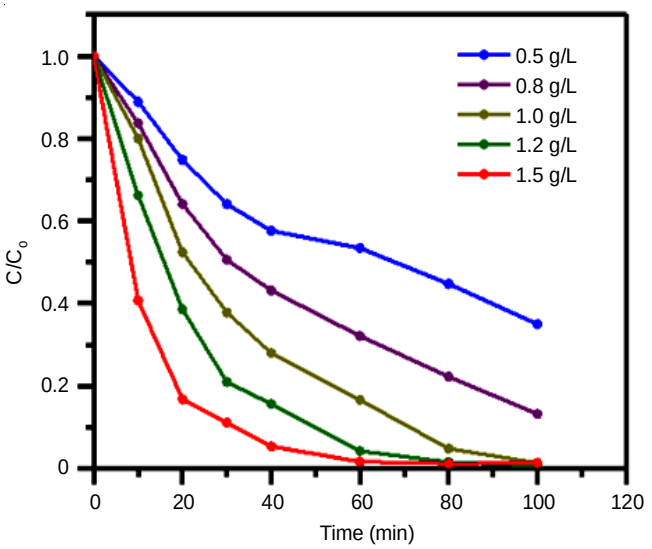

Fig. 5. Photocatalytic degradation of rhodamine B dye when the doses of Sn doped CeO_2-Fe_2O_3 catalyst was varied from 0.5 to 1.5 g/L

Further, the degradation of rhodamine B dye with Sn doped CeO_2-Fe_2O_3 was investigated by the change in the pH of the dye solution, while the concentration of dye and catalyst

remained constant. Fig. 6 shows the change in the degradation rate of rhodamine B dye by the effect of pH change. Here it can be observed that when the pH of the solution was 2 then the degradation of the dye reached up to 20% only. But when the pH of the reaction solution increased from 2 to 10, the degradation rate continuously increased from 20% to 99% [46,47]. This shows that the degradation efficiency is directly proportional to the basic pH of the dye solution.

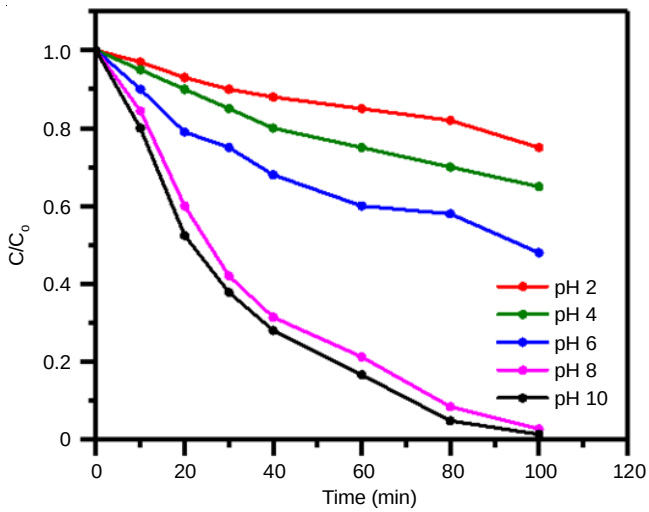

Fig. 6. Photocatalytic degradation of rhodamine B dye at different solution pH by using Sn doped CeO_2-Fe_2O_3

The COD tests were performed to ensure the complete degradation and removal of the rhodamine B dye from the solution. Fig. 7 represents the COD removal of the rhodamine B dye as a function of reaction time. Here, one can see that the initial solution of rhodamine B dye shows the 0% COD removal [48]. After 10 min, the COD of the reaction is removed up to 20%, which shows the progress of the degradation reaction under sunlight. As the reaction progressed, the COD of the reaction was continuously removed from the solution. At the end of the reaction, the COD removal up to 98% after 100 min of the reaction was observed, which supports the degradation of rhodamine B dye by Sn doped CeO_2-Fe_2O_3.

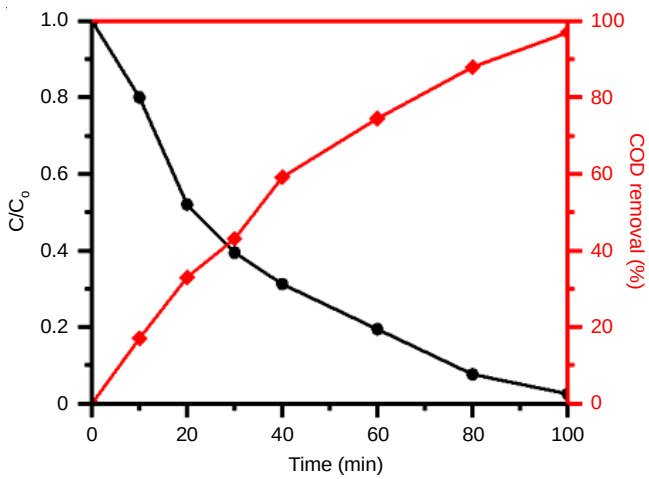

Fig. 7. Degradation of rhodamine B and COD removal from the solution by using Sn doped CeO_2-Fe_2O_3 under sunlight

Next, the complete degradation and removal of rhodamine B dye from solution with Sn doped CeO_2-Fe_2O_3 photocatalyst were further ensured by HPLC analysis [49,50]. Fig. 8 shows the HPLC chromatograms of the degradation reactions recorded at different time intervals starting from 0 min to 100 min during the photocatalytic process. In Fig. 8, the chromatogram present at 0 min shows the peaks at 7.7 min, which corresponded to the characteristic peaks of pure rhodamine B dye. Thereafter, as the reaction time increases, the peak at 7.7 min starts to decrease, which indicates the degradation of rhodamine B dye has begun. This peak further decreases continuously in the next chromatograms and at 100 min, this peak is almost diminished, which represents the removal of the rhodamine B dye from the solution. Besides this, the chromatogram at 10 min shows the rise of new peaks at 4.4, 5.6 and 6.6 min apart from 7.7 min. These new peaks arise due to the formation of degraded products of rhodamine B dye from the photocatalytic degradation process. These peaks first started to grow as the reaction time increased, but after a certain time, these peaks also started to decrease and diminished at the end. The last chromatogram shows, there are no peaks present here; it proves the complete removal of rhodamine B dye and its degraded products from the dye solution.

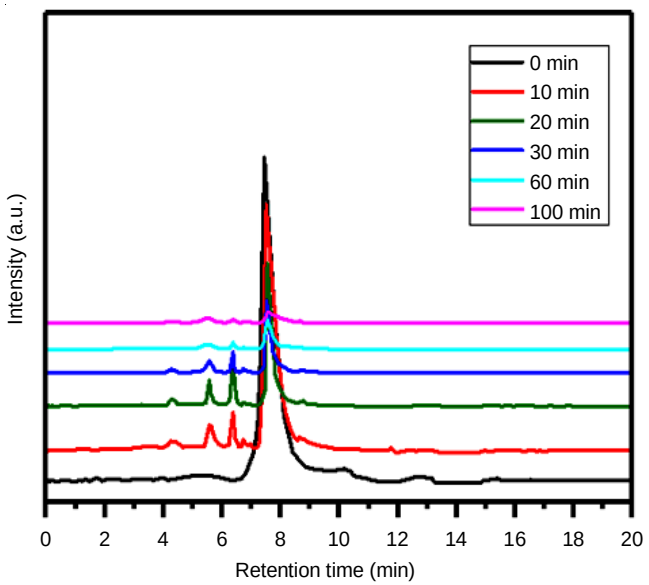

Fig. 8. HPLC chromatogram of degradation and removal of rhodamine B from the solution by using Sn doped CeO_2-Fe_2O_3 under sunlight

The catalyst was further tested for reusability and stability. For this purpose, cyclic tests were performed (Fig. 9). The same catalyst was used for the cyclic test and four consecutive cycles were performed [48]. The Sn doped CeO_2-Fe_2O_3 photocatalyst was found to degrade up to 95% of dye from the solution till the last cycle. This proves the high degradation efficiency of the Sn doped CeO_2-Fe_2O_3 photocatalyst, which can be used at the industrial level usage.

Mechanism: To understand the reaction mechanism, the reactive species involved in the degradation process were identified by performing scavenger tests. For this purpose, 1 mM of different scavengers was added to the reaction beaker before

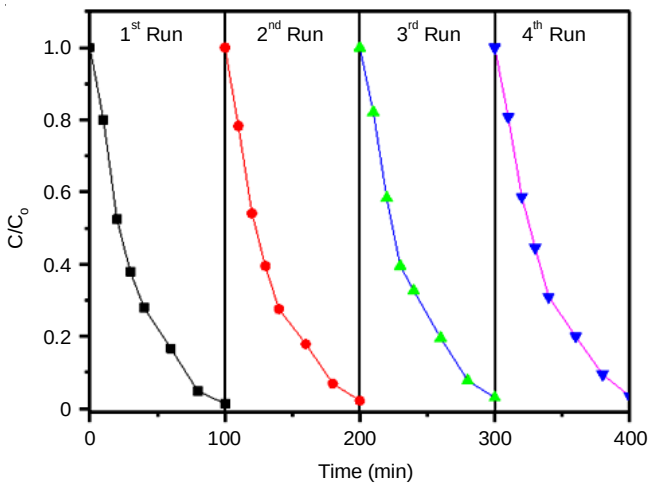

Fig. 9. Degradation of rhodamine B dye with Sn doped CeO_2-Fe_2O_3 catalyst up to four successive cycles under sunlight irradiation

the sunlight exposure. The scavengers used are benzoquinone (BQ) for $O_2^{\bullet-}$, ammonium oxalate (AO) for h^+ and *tert*-butanol (*t*-BuOH) for $^{\bullet}OH$ scavenging [48]. The scavenger study shows that the addition of BQ and *t*-BuOH to the reaction beaker reduced the rate of degradation reaction, while the addition of AO does not affect the degradation rate (Fig. 10). The inhibition of the degradation reaction due to BQ and *t*-BuOH shows the active role of $O_2^{\bullet-}$ and $^{\bullet}OH$ radical species. Fig. 10 shows that in the presence of $O_2^{\bullet-}$ quencher (BQ), the reaction proceeds up to 24% only while in the presence of $^{\bullet}OH$ radical quencher (*t*-BuOH), the reaction proceeds only 10%. Besides this, in the presence of h^+ quencher (AO), reaction completes up to 98%. So, the $O_2^{\bullet-}$ and $^{\bullet}OH$ radicals are generating during photocatalysis and leading to the degradation of the rhodamine B dye.

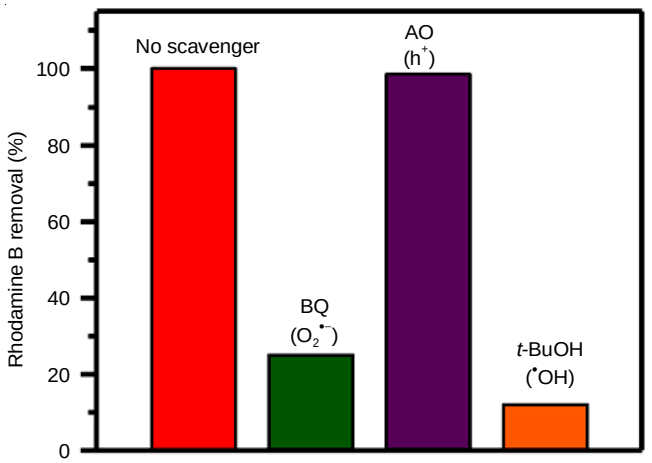

Fig. 10. Scavengers studies to understand the on the photocatalytic degradation of rhodamine B (RhB) dye by using scavengers, BQ, *t*-BuOH, AO under sunlight with Sn doped CeO_2-Fe_2O_3

The mechanism of degradation of dye solution by photocatalyst was studied (Fig. 11). The mechanism of photocatalytic degradation of rhodamine B dye is mainly dependent on the bandgap of the catalyst and the availability of surface charge carriers. The reported band gap of CeO_2 is 3.1 eV and Fe_2O_3 is

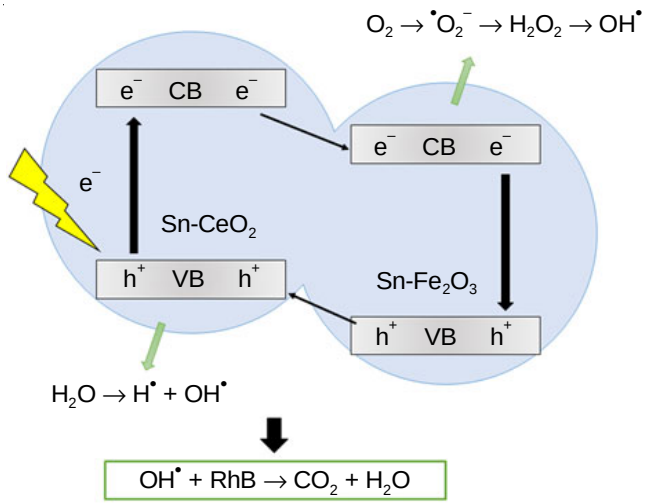

Fig. 11. Schematic diagram representing the photocatalytic degradation of rhodamine B (RhB) dye with Sn doped CeO_2-Fe_2O_3 catalyst under sunlight irradiation

2.3 eV [45,52]. In this report, a composite system of CeO_2 and Fe_2O_3 is prepared and the new band gap value obtained is 2.4 eV. And, after the doping of Sn in the CeO_2-Fe_2O_3 system, the band gap values were modified and the value obtained was 2.21 eV. The modified band gap is reaching the values where a compound is a visible active catalyst. In the composite, some of the Ce^{4+} lattice sites are occupied by Sn^{4+} ions and leads to the formation of Ce-O-Sn/Fe_2O_3 heterojunction, which facilitates the migration of the electrons and lower the electron-hole recombination rate [49]. When the catalyst and dye suspension is irradiated by sunlight, then generated electrons move to the conduction band (CB) of Sn-CeO_2 from the valance band (VB) of Sn-CeO_2. Due to the transfer of the electrons, positively charged holes are generated in the VB (Sn-CeO_2). The photogenerated electrons then transferred to CB (Sn-Fe_2O_3) from CB (Sn-CeO_2) and further moved to VB (Sn-Fe_2O_3). From here, electrons go to VB (Sn-CeO_2) and completes a cycle.

The photo-generated electrons will react with oxygen present in the dye solution and generate the $O_2^{\bullet-}$ radical. These $O_2^{\bullet-}$ radicals will react with water molecules and form H_2O_2 which will further generate $^{\bullet}OH$ radicals (Fig. 11). On the other hand, the photogenerated holes will react with water molecules present in the solution and produce $^{\bullet}H$ and $^{\bullet}OH$ radicals. These generated $^{\bullet}OH$ radicals will further react with rhodamine B dye and degrade it into CO_2 and H_2O molecules [53].

Conclusion

In this report, Sn doped CeO_2-Fe_2O_3 nanocomposite was prepared by using a simple thermal decomposition method and the catalyst was applied to degrade rhodamine B dye under the sunlight. The XRD analysis of catalyst indicates the well incorporation of the Sn into the structure with a shift towards the high 2θ value. The FESEM image shows the sphere-shaped morphology with varying sizes of 1-2 mm. The BET analysis of Sn doped CeO_2-Fe_2O_3 and CeO_2-Fe_2O_3 composite showed a surface area of 24.4 and 17 m^2/g, respectively. The band gap of catalyst was narrowed from 2.4 eV to 2.21 eV after the Sn doping into the CeO_2-Fe_2O_3 composite. The synthesized Sn

doped CeO_2-Fe_2O_3 catalyst showed an improved degradation efficiency than the CeO_2-Fe_2O_3 catalyst. The catalyst showed complete removal of rhodamine B dye within 100 min of reaction time under sunlight irradiation. The degradation efficiency of the photocatalyst was tested by the effect of doses of catalyst and pH under sunlight. The reusability of Sn doped photocatalyst was tested up to four consecutive cycles and the catalyst was found very active till the fourth cycle. A mechanism for the degradation of rhodamine B dye is proposed with the transfer of the charge. The COD removal test confirmed the degradation and removal of rhodamine B dye from the dye solution by photocatalyst and HPLC data also supports the complete removal of the dye.

ACKNOWLEDGEMENTS

The authors are grateful to "Genesis of Chemistry" for providing necessary facilities and support.

CONFLICT OF INTEREST

The authors declare that there is no conflict of interests regarding the publication of this article.

REFERENCES

1. A. Molla, M. Sahu and S. Hussain, *J. Mater. Chem. A Mater. Energy Sustain.*, **3**, 15616 (2015); https://doi.org/10.1039/C5TA02888D
2. V.S. Talismanov, S.V. Popkov, O.G. Karmanova, S.S. Zykova, M.V. Shustov, L.A. Zhuravleva and N.G. Tokareva, *Rasayan J. Chem.*, **14**, 1711 (2021); http://doi.org/10.31788/RJC.2021.1436537
3. K. Kasinathan, J. Kennedy, M. Elayaperumal, M. Henini and M. Malik, *Sci. Rep.*, **6**, 38064 (2016); https://doi.org/10.1038/srep38064
4. X. Yang, Z. Chen, J. Xu, H. Tang, K. Chen and Y. Jiang, *ACS Appl. Mater. Interfaces*, **7**, 15285 (2015); https://doi.org/10.1021/acsami.5b02649
5. B. Viswanathan, *CCAT*, **7**, 99 (2018); https://doi.org/10.2174/2211544707666171219161846
6. G.V. Tsaplin, S.S. Grishin, E.P. Baberkina, S.V. Popkov, V.S. Talismanov, O.G. Karmanova and S.S Zykova, *Rasayan J. Chem.*, **14**, 1816 (2021); http://doi.org/10.31788/RJC.2021.1436574
7. R. Singh, *J. Civil Eng. Environ. Sci.*, **7**, 8 (2021); https://doi.org/10.17352/2455-488X.000039
8. H.A. Kiwaan, T.M. Atwee, E.A. Azab and A.A. El-Bindary, *J. Mol. Struct.*, **1200**, 127115 (2020); https://doi.org/10.1016/j.molstruc.2019.127115
9. C.-Y. Chen, *Water Air Soil Pollut.*, **202**, 335 (2009); https://doi.org/10.1007/s11270-009-9980-4
10. S. Luo, R. Wang, J. Yin, T. Jiao, K. Chen, G. Zou, L. Zhang, J. Zhou, L. Zhang and Q. Peng, *ACS Omega*, **4**, 3946 (2019); https://doi.org/10.1021/acsomega.9b00231
11. S. Li, Q. Lin, X. Liu, L. Yang, J. Ding, F. Dong, Y. Li, M. Irfan and P. Zhang, *RSC Adv.*, **8**, 20277 (2018); https://doi.org/10.1039/C8RA03117G
12. M. Umadevi, R. Rathinam, S. Poornima, T. Santhi and S. Pattabhi, *Asian J. Chem.*, **33**, 1919 (2021); https://doi.org/10.14233/ajchem.2021.23330
13. R. Rathinam and M. Govindaraj, *Nat. Environ. Pollut. Technol.*, **20**, 1069 (2021); https://doi.org/10.46488/NEPT.2021.v20i03.014
14. R. Singh, M. Singh, N. Kumari, S. Janak, S. Maharana and P. Maharana, *J. Compos. Sci.*, **5**, 162 (2021); https://doi.org/10.3390/jcs5060162
15. R. Rathinam and S. Pattabhi, *Indian J. Ecol.*, **46**, 167 (2019).
16. T.M. Breault and B.M. Bartlett, *J. Phys. Chem. C*, **116**, 5986 (2012); https://doi.org/10.1021/jp2078456
17. Y.-H. Chiu, T.-F.M. Chang, C.-Y. Chen, M. Sone and Y.-J. Hsu, *Catalysts*, **9**, 430 (2019); https://doi.org/10.3390/catal9050430
18. R. Singh, Eds.: A. Patnaik, E. Kozeschnik, V. Kukshal, Advancements in Energy Storage through Graphene. In: Advances in Materials Processing and Manufacturing Applications. iCADMA 2020. Lecture Notes in Mechanical Engineering. Springer, Singapore (2021).
19. V. Alwera, S. Sehlangia and S. Alwera, *Sep. Sci. Technol.*, **56**, 2278 (2021); https://doi.org/10.1080/01496395.2020.1819826
20. R. Singh, N. Kaur and M. Singh, *Mater. Today Proc.*, **44**, 242 (2021); https://doi.org/10.1016/j.matpr.2020.09.461
21. R. Singh, A. Altaee and S. Gautam, *Heliyon*, **6**, e04487 (2020); https://doi.org/10.1016/j.heliyon.2020.e04487
22. R.S. Sabry, M.I. Rahmah and W.J. Aziz, *J. Mater. Sci. Mater. Electron.*, **31**, 13382 (2020); https://doi.org/10.1007/s10854-020-03893-8
23. Z.N. Kayani, A. Usman, H. Nazli, R. Sagheer, S. Riaz and S. Naseem, *Appl. Phys., A Mater. Sci. Process.*, **126**, 559 (2020); https://doi.org/10.1007/s00339-020-03748-3
24. D. Majumder, I. Chakraborty, K. Mandal and S. Roy, *ACS Omega*, **4**, 4243 (2019); https://doi.org/10.1021/acsomega.8b03298
25. D. Channei, A. Nakaruk, P. Jannoey and S. Phanichphant, *Solid State Sci.*, **87**, 9 (2019); https://doi.org/10.1016/j.solidstatesciences.2018.10.016
26. Z.M. Yang, G.F. Huang, W.Q. Huang, J.M. Wei, X.G. Yan, Y.Y. Liu, C. Jiao, Z. Wan and A. Pan, *J. Mater. Chem. A Mater. Energy Sustain.*, **2**, 1750 (2014); https://doi.org/10.1039/C3TA14286H
27. N. Wetchakun, S. Chaiwichain, B. Inceesungvorn, K. Pingmuang, S. Phanichphant, A.I. Minett and J. Chen, *ACS Appl. Mater. Interfaces*, **4**, 3718 (2012); https://doi.org/10.1021/am300812n
28. S. Hu, F. Zhou, L. Wang and J. Zhang, *Catal. Commun.*, **12**, 794 (2011); https://doi.org/10.1016/j.catcom.2011.01.027
29. A. Krishnan, S. Beena and M. Chandran, *Mater. Today Proc.*, **18**, 4968 (2019); https://doi.org/10.1016/j.matpr.2019.07.489
30. H. Liu, H.K. Shon, X. Sun, S. Vigneswaran and H. Nan, *Appl. Surf. Sci.*, **257**, 5813 (2011); https://doi.org/10.1016/j.apsusc.2011.01.110
31. A.I. Ahmed S.M. Hassan and M.A. Mannaa, *J. Sci.: Adv. Mater. Dev.*, **4**, 400 (2019); https://doi.org/10.1016/j.jsamd.2019.06.004
32. M. Sohail, N. Baig, M. Sher, R. Jamil, M. Altaf, S. Akhtar and M. Sharif, *ACS Omega*, **5**, 6405 (2020); https://doi.org/10.1021/acsomega.9b03876
33. S. Alwera and R. Bhushan, *Biomed. Chromatogr.*, **31**, e3983 (2017); https://doi.org/10.1002/bmc.3983
34. V. Alwera, S. Sehlangia and S. Alwera, *J. Liq. Chromatogr. Rel. Technol.*, **43**, 742 (2020); https://doi.org/10.1080/10826076.2020.1798250
35. A. Krishnan and S.M. Aboobakar Shibli, *Ind. Eng. Chem. Res.*, **57**, 16217 (2018); https://doi.org/10.1021/acs.iecr.8b03692
36. T.C. Bhagya, A. Krishnan, A.R. S, A.S. M, B.R. Sreelekshmy, P. Jineesh and S.M.A. Shibli, *Photochem. Photobiol. Sci.*, **18**, 1716 (2019); https://doi.org/10.1039/C9PP00119K
37. S. Alwera and R. Bhushan, *Biomed. Chromatogr.*, **30**, 1772 (2016); https://doi.org/10.1002/bmc.3752
38. S. Alwera and R. Bhushan, *J. Liq. Chromatogr. Rel. Technol.*, **40**, 707 (2017); https://doi.org/10.1080/10826076.2017.1348954
39. M.R. Abhilash, G. Akshatha and S. Srikantaswamy, *RSC Adv.*, **9**, 8557 (2019); https://doi.org/10.1039/C8RA09929D

40. A. Krishnan, M.A. Sha, R. Basheer, A.H. Riyas and S.M.A. Shibli, *Mater. Sci. Semicond. Process.*, **116**, 105138 (2020); https://doi.org/10.1016/j.mssp.2020.105138
41. J. Cao, Y. Zhu, L. Shi, L. Zhu, K. Bao, S. Liu and Y. Qian, *Eur. J. Inorg. Chem.*, **2010**, 1172 (2010); https://doi.org/10.1002/ejic.200901116
42. L.-C. Chen, Y.-J. Tu, Y.-S. Wang, R.-S. Kan and C.-M. Huang, *J. Photochem. Photobiol. Chem.*, **199**, 170 (2008); https://doi.org/10.1016/j.jphotochem.2008.05.022
43. H. Lahmar, M. Benamira, S. Douafer, L. Messaadia, A. Boudjerda and M. Trari, *Chem. Phys. Lett.*, **742**, 137132 (2020); https://doi.org/10.1016/j.cplett.2020.137132
44. V. Eskizeybek, F. Sari, H. Gülce, A. Gülce and A. Avci, *Appl. Catal. B*, **119-120**, 197 (2012); https://doi.org/10.1016/j.apcatb.2012.02.034
45. S. Prabhu, T. Viswanathan, K. Jothivenkatachalam and K. Jeganathan, *Int. J. Mater. Sci.*, **2014**, 536123 (2014); https://doi.org/10.1155/2014/536123
46. A. Boughelout, R. Macaluso, M. Kechouane and M. Trari, *React. Kinet. Mech. Catal.*, **129**, 1115 (2020); https://doi.org/10.1007/s11144-020-01741-8
47. H. Anwer, A. Mahmood, J. Lee, K.-H. Kim, J.-W. Park and A.C.K. Yip, *Nano Res.*, **12**, 955 (2019); https://doi.org/10.1007/s12274-019-2287-0
48. V. Alwera, S. Singh, V.C. Srivastava and T.K. Mandal, *ChemistrySelect*, **5**, 4674 (2020); https://doi.org/10.1002/slct.202000298
49. S. Alwera, V. Alwera and S. Sehlangia, *Biomed. Chromatogr.*, **34**, e4943 (2020); https://doi.org/10.1002/bmc.4943
50. S. Alwera and R. Bhushan, *Biomed. Chromatogr.*, **30**, 1223 (2016); https://doi.org/10.1002/bmc.3671
51. S. Alwera, *ACS Sustain. Chem.& Eng.*, **6**, 11653 (2018); https://doi.org/10.1021/acssuschemeng.8b01869
52. J. Bandara, U. Klehm and J. Kiwi, *Appl. Catal. B*, **76**, 73 (2007); https://doi.org/10.1016/j.apcatb.2007.05.007
53. R. Zha, R. Nadimicherla and X. Guo, *J. Mater. Chem. A Mater. Energy Sustain.*, **3**, 6565 (2015); https://doi.org/10.1039/C5TA00764J